On New Convolutional Neural Network Based Algorithms for Selective Segmentation of Images

Liam Burrows[1], Ke Chen[1(✉)], and Francesco Torella[2]

[1] Department of Mathematical Sciences and Centre for Mathematical Imaging Techniques, University of Liverpool, Liverpool, UK
k.chen@liv.ac.uk

[2] Liverpool Vascular and Endovascular Service, Liverpool University Hospitals, Liverpool L7 8XP, UK
http://www.liv.ac.uk/~cmchenke

Abstract. Selective segmentation is an important aspect of image processing. Being able to reliably segment a particular object in an image has important applications particularly in medical imaging. Robust methods can aid clinicians with diagnosis, surgical planning, etc. Many selective segmentation algorithms use geometric constraints such as information from the edges in order to determine where an object lies. It is still a challenge where there is low contrast present between two objects, and an edge is difficult to detect. Relying on purely edge constraints in this case will fail. We aim to make use of area constraints in addition to edge information in a segmentation model which is robustly capable of segmenting regions in an image even in the presence of low contrast, when given suitable user input. In addition, we implement a deep learning algorithm based on this model, allowing for a supervised, semi-supervised or unsupervised approach, depending on data availability.

Keywords: Image segmentation · Variational model · Deep learning

1 Introduction

Image segmentation has many important applications in medical imaging, providing a tool for clinicians to assist with diagnosis, monitoring, surgical planning etc. Variational methods have been well studied over the past few decades, the first major contribution was by Mumford and Shah [12], who proposed a region based method involving segmentation by approximating an input image. Another important region based approach is the piecewise constant two-phase version of the Mumford-Shah method by Chan and Vese [6]. A second approach for segmentation are edge based methods, such as the active contour method proposed by Kass et al. [10], which was further developed by Caselles et al. in the Geodesic

Active Contours model (GAC) [4]. These edge based approaches involve driving an active contour from an initial point, aiming to segment an object by stopping it at an edge, making use of an edge detector.

Although image segmentation is a widely studied subject, there exist many open challenges. First, no models are yet capable to segment any given image (i.e. without assumption of the underlying images and its quality). Second, few models in particular aim for selective segmentation. Third, many variational models are non-convex which make both the theory and algorithm challenging. Fourth, many important applications cannot provide sufficient training data for leaning models. This paper addresses the task of selective segmentation and developing leaning algorithms that do not rely on a large training set of data.

Selective segmentation is of particular importance in medical imaging, as often we are only interested in a particular object (or objects) of interest. Most variational selective segmentation methods take a hybrid approach, combining both region and edge based methods to impose geometrical constraints on a particular region of interest. In 2005, Gout et al. [8] adopted the GAC model, making use of some marker points $\mathcal{M}$, typically input by the user, to indicate the region of interest. This was further adapted by Badshah and Chen [1], who added region information in the form of the contribution by Chan-Vese [6]. Rada and Chen [14] introduced area constraints to the Badshah-Chen method in order to increase reliability. The aim was to impose a constraint on the area of the region inside the contour, by ensuring that the area was close to that of the area of the region defined by the user.

In 2015, Spencer and Chen [18] introduced a model making use of the Euclidean distance as a standalone term, giving more control over the distance constraint by tuning the parameter in front. This method provides good results however is dependent on the placement of $\mathcal{M}$ and sensitive to parameter selection. Most recently, Roberts and Chen [15] proposed to replace the Euclidean distance with a Geodesic distance, which increases when an edge is detected, providing a much more intuitive distance constraint for selective segmentation.

The Roberts-Chen model provides a robust framework to selectively segment objects, particularly where edges are well defined. It is still a difficult challenge to segment an object where edges aren't well defined and low contrast is present. The authors in [15] provide a solution in the form of "antimarkers", which allow the user to indicate unwanted regions, but this requires more user interaction, which we would prefer to minimise. An alternate approach is to use edge enhancement ideas as in [3], however this is a time consuming preprocess.

In this work, we consider merging the Roberts-Chen model with the area constraint idea from Rada and Chen in order to maximize the benefit of the given marker set $\mathcal{M}$ and to reduce the reliance on just edge information. The area constraint allows us to impose a penalty in the case that an edge is weak or unable to be detected by the geodesic distance. In the original work from Rada and Chen [14], they proposed a non-convex approach using level sets so a global minimiser is not assumed. This paper (i) reformulates the Rada model to

a relaxed version so that a proof of convexity can be given, and (ii) implements a deep learning algorithm based on this new model.

2   Related Works

In this section we will review some related works. Let $\Omega \subset \mathbb{R}^2$ be a bounded image domain, with image z defined on Ω. We will focus on two-phase models, so that our region of interest is denoted as Ω_1, and the background is denoted by $\Omega_2 = \Omega \backslash \Omega_1$. The task of these variational segmentation methods is to find the contour Γ which separates Ω_1 and Ω_2.

In the following we review the Rada-Chen model [14], which is based on the framework of Chan-Vese [6]. This method makes use of a marker set $\mathcal{M}$ input by the user. Formally, this is a set of n points defined as $\mathcal{M} = \{\mathbf{x}_i \in \Omega, i = 1, ..., n\}$. The Rada-Chen model takes the following form:

$$\min_{\Gamma, c_1, c_2} \Big\{ \text{Length}(\Gamma) + \lambda_1 \int_{\Omega_1} (z - c_1)^2 d\mathbf{x} + \lambda_2 \int_{\Omega_2} (z - c_2)^2 d\mathbf{x}$$
$$+ \xi \Big(\Big(\int_{\Omega_1} d\mathbf{x} - A_1 \Big)^2 + \Big(\int_{\Omega_2} d\mathbf{x} - A_2 \Big)^2 \Big) \Big\}, \qquad (1)$$

where c_1 and c_2 are the average intensities of z inside and outside of Γ respectively, and A_1 is the area of the polygon defined by $\mathcal{M}$, and $A_2 = 1 - A_1$.

In order to solve this, the level and set idea from [13] is used. In this way, we can represent our contour Γ in terms of a level set φ such that:

$$\begin{cases} \Gamma = \{\mathbf{x} \in \Omega | \varphi(\mathbf{x}) = 0\} \\ \text{in}(\Gamma) = \{\mathbf{x} \in \Omega | \varphi(\mathbf{x}) > 0\} \\ \text{out}(\Gamma) = \{\mathbf{x} \in \Omega | \varphi(\mathbf{x}) < 0\}. \end{cases} \qquad (2)$$

The Rada-Chen model reformulated in terms of a level set is given by:

$$\min_{\varphi, c_1, c_2} \Big\{ \int_{\Omega} g |\nabla H_\epsilon(\varphi)| d\mathbf{x} + \lambda \int_{\Omega} (z - c_1)^2 H_\epsilon(\varphi) + (z - c_2)^2 (1 - H_\epsilon(\varphi)) d\mathbf{x}$$
$$+ \xi \Big(\Big(\int_{\Omega} H_\epsilon(\varphi) d\mathbf{x} - A_1 \Big)^2 + \Big(\int_{\Omega} (1 - H_\epsilon(\varphi)) d\mathbf{x} - A_2 \Big)^2 \Big) \Big\}, \qquad (3)$$

where we have set $\lambda = \lambda_1 = \lambda_2$, $H_\epsilon(\varphi) = \frac{1}{2}(1 + \frac{2}{\pi} \arctan(\frac{\varphi}{\epsilon}))$ is the regularised Heaviside function, and $g = g(|\nabla z|)$ is an edge detector given by $g(s) = \frac{1}{1 + \iota |\nabla z|^2}$.

The final term of the Rada-Chen model enforces a penalty on the area inside the contour Γ, so that the area inside Γ has a similar area to A_1. This encourages the output of the model to be selective, however there is no location information to put a penalty on the contour from evolving far away from $\mathcal{M}$. A potential result is that the output contour can be disconnected over the whole image domain with the sum of its area similar to A_1, but not necessarily close to $\mathcal{M}$.

In 2015, Spencer and Chen [18] introduced a stand-alone distance term making use of the Euclidean distance, and also reformulating their model from a non-convex version using Heavisides and level sets, to a convex-relaxed version using the ideas from [5]. Later, Roberts and Chen [15] replaced the Euclidean distance with Geodesic distance, so that their model is as follows:

$$\min_{u,c_1,c_2} \int_\Omega g|\nabla u| \, d\mathbf{x} + \lambda \int_\Omega ((z - c_1)^2 - (z - c_2)^2)u \, d\mathbf{x}$$
$$+ \alpha \int_\Omega \nu(u) \, d\mathbf{x} + \theta \int_\Omega \mathcal{D}_G u \, d\mathbf{x}, \tag{4}$$

where $\nu(u)$ is a penalty term to encourage the output u to be constraint between $[0, 1]$. $\mathcal{D}_G$ is the Geodesic distance, which puts a penalty on regions away from $\mathcal{M}$.

The Geodesic distance from $\mathcal{M}$ was introduced in [15] and involves solving the following Eikonal equation:

$$\begin{cases} |\nabla \mathcal{D}_G(\mathbf{x})| = \epsilon_G + \beta_G |\nabla z(\mathbf{x})| + \theta_G \mathcal{D}_E, & \mathbf{x} \in \Omega \\ \mathcal{D}_G(\mathbf{x}) = 0, & \mathbf{x} \in \mathcal{M}, \end{cases} \tag{5}$$

where $\mathcal{D}_E$ is the Euclidean distance from $\mathcal{M}$. This can be solved quickly using fast marching [17], or fast sweeping [20] methods, for example.

The model using the Geodesic distance is robust to user input, and provides excellent results for segmenting images in which the edges are well defined. A single click for relatively simple objects will usually suffice, and in comparison to other models, the geodesic distance requires less input usually. In [15], the authors discuss potential problems such as noise in an image (it is suggested that we smooth the image z before solving the system (5) and low contrast, to which a solution is proposed involving using a second set of markers, called anti-markers, to indicate unwanted regions and put an appropriate penalty on them. While this can be a solution, this requires more user input.

Overall, the geodesic distance is a good penalty, however it can be tricky to tune the smoothing appropriately to remove noise, but to also preserve sensitive edges in regions of low contrast. Therefore, in the next section, we pair up the area constraint from Rada-Chen [14] with the geodesic distance from Roberts-Chen [15] to both restrict the segmentation result from evolving far from $\mathcal{M}$, and to also restrict it from evolving too much from the input area.

3   Proposed Model

In this section we propose a new model, which uses both the geodesic distance and an area constraint, and minimises the following functional:

$$F(u) = \int_\Omega g|\nabla u|d\mathbf{x} + \lambda \int_\Omega ((z - c_1)^2 - (z - c_2)^2)ud\mathbf{x} + \alpha \int_\Omega \nu(u)d\mathbf{x}$$
$$+ \frac{\xi}{2}\Big(\int_\Omega ud\mathbf{x} - A_1\Big)^2 + \theta \int_\Omega \mathcal{D}_G ud\mathbf{x}. \tag{6}$$

Our area constraint puts a penalty on the area of the region inside Γ. This is simpler, but equivalent to the area constraint in (3).

In the following we provide a proof that each term is convex.

$$F(u) = TV_g(u) + f(u) + r(u) \tag{7}$$

where $TV_g(u) = \int_\Omega g|\nabla u|d\mathbf{x}$, $f(u) = \lambda \int_\Omega ((z-c_1)^2-(z-c_2)^2)ud\mathbf{x}+\theta \int_\Omega \mathcal{D}_G ud\mathbf{x}+\alpha \int_\Omega \nu(u)d\mathbf{x}$ and $r(u) = \frac{\xi}{2}\left(\int_\Omega ud\mathbf{x} - A_1\right)^2$. It is known from [15, 18] that $f(u)$ is convex, and an explicit proof can be found in [9] for the convexity of the $TV_g(u)$ term. Therefore we give a proof that the area constraint term is fully convex. To prove convexity we consider $\phi \in [0,1]$ to be a constant, and the following to hold $\forall u_1, u_2$:

$$
\begin{aligned}
r(\phi u_1 + (1 - \phi)u_2) &= \left(\int_\Omega (\phi u_1 + (1 - \phi)u_2)d\mathbf{x} - A_1\right)^2 \\
&= \left(\phi \int_\Omega u_1 d\mathbf{x} + (1 - \phi)\int_\Omega u_2 d\mathbf{x} - A_1\right)^2 \\
&\leq \left(\phi \int_\Omega u_1 d\mathbf{x} - A_1\right)^2 + \left((1 - \phi)\int_\Omega u_2 d\mathbf{x} - A_1\right)^2 \\
&= \phi^2 r(u_1) + (1 - \phi)^2 r(u_2) \\
&\leq \phi r(u_1) + (1 - \phi)r(u_2).
\end{aligned}
$$

Therefore, for fixed c_1 and c_2, the model given in (6) is clearly fully convex, thus a global minimizer is guaranteed and our output is not dependent on the initialisation.

Numerical Algorithm

Minimising the functional (6) using the Euler-Lagrange equation with respect to u yields the following system:

$$\nabla \cdot \left(g\frac{\nabla u}{|\nabla u|}\right) - f = 0, \ \mathbf{x} \in \Omega, \qquad \frac{\partial u}{\partial n} = 0, \ \mathbf{x} \in \partial\Omega,$$

where $f = \lambda\left((z - c_1)^2 - (z - c_2)^2\right) + \alpha\nu'(u) + \xi\left(\int_\Omega ud\mathbf{x} - A_1\right) + \theta\mathcal{D}_G$.

We use the gradient descent method to solve the above system, given by:

$$\frac{\partial u}{\partial t} = \nabla \cdot (G\nabla u) - f,$$

where $G = \frac{g}{|\nabla u|}$. To solve this, an additive operator splitting (AOS) method is used [11, 19], which is an efficient, semi-implicit method, allowing for larger time steps which still ensuring stability in the numerical scheme. To account for the instability introduced by the penalty term $\nu'(u)$, we use the improved AOS2 method introduced in [18].

4   Deep Learning Algorithms

While numerically solving our model can provide accurate results, it can be time consuming to solve. In addition to solving the model, we can implement our method into a learning algorithm. We can take three separate approaches to this: supervised, semi-supervised and unsupervised. Suppose we have N total training images, and let $u_W(z, \mathbb{M})$ be the output of our network with weights W and input z, with $\mathbb{M}$ defined as the polygon formed by $\mathcal{M}$. In the following we denote $u^{(j)}$ as $u^{(j)} = u_W(z^{(j)}, \mathbb{M}^{(j)})$.

1. **Supervised Algorithm:** Using a supervised approach, we can take our functional and use it as a loss function. We can make use of ground truth labels in the fidelity term as done in [7], as follows:

$$
\mathcal{L}_S(W) = \sum_{j=1}^{N} \int_\Omega g^{(j)} |\nabla u^{(j)}| d\mathbf{x} + \lambda \int_\Omega ((v^{(j)} - c_1^S)^2 - (v^{(j)} - c_2^S)^2) u^{(j)} d\mathbf{x}
$$
$$
+ \frac{\xi}{2} \Big(\int_\Omega u^{(j)} d\mathbf{x} - A_1^{(j)} \Big)^2 + \theta \int_\Omega \mathcal{D}_G^{(j)} u^{(j)} d\mathbf{x}, \tag{8}
$$

   $v^{(j)}$ are the ground truth labels, and c_1^S and c_2^S are 1 and 0 respectively (as $v^{(j)}$ is 1 and 0 inside and outside Γ respectively.)

2. **Unsupervised Algorithm:** If ground truth labels aren't available, we can implement an unsupervised approach by using the image in the fidelity, as done in the classical approach:

$$
\mathcal{L}_{US}(W) = \sum_{j=1}^{N} \int_\Omega g^{(j)} |\nabla u^{(j)}| d\mathbf{x} + \lambda \int_\Omega ((z^{(j)} - c_1^{(j)^{US}})^2 - (z^{(j)} - c_2^{(j)^{US}}) u^{(j)} d\mathbf{x}
$$
$$
+ \frac{\xi}{2} \Big(\int_\Omega u^{(j)} d\mathbf{x} - A_1^{(j)} \Big)^2 + \theta \int_\Omega \mathcal{D}_G^{(j)} u^{(j)} d\mathbf{x}, \tag{9}
$$

   where $c_1^{(j)^{US}}$ and $c_1^{(j)^{US}}$ are fixed to be the average intensity inside and outside $\mathbb{M}$, defined as:

$$
c_1^{(j)^{US}} = \frac{\int_\Omega z^{(j)} \mathbb{M}^{(j)} d\mathbf{x}}{\int_\Omega \mathbb{M}^{(j)} d\mathbf{x}}, \quad c_2^{(j)^{US}} = \frac{\int_\Omega z^{(j)} (1 - \mathbb{M}^{(j)}) d\mathbf{x}}{\int_\Omega (1 - \mathbb{M}^{(j)}) d\mathbf{x}}
$$

3. **Semi-supervised Algorithm:** If ground truth labels are available for only a select few, we can use a combination of the supervised and unsupervised:

$$
\mathcal{L}_{SS}(W) = \sum_{j=1}^{N} \int_\Omega g^{(j)} |\nabla u^{(j)}| d\mathbf{x} + \frac{\xi}{2} \Big(\int_\Omega u^{(j)} d\mathbf{x} - A_1^{(j)} \Big)^2 + \theta \int_\Omega \mathcal{D}_G^{(j)} u^{(j)} d\mathbf{x}
$$
$$
+ \sum_{j=1}^{N_1} \lambda \int_\Omega ((v^{(j)} - c_1^S)^2 - (v^{(j)} - c_2^S)^2) u^{(j)} d\mathbf{x}
$$
$$
+ \sum_{j=N_1+1}^{N} \lambda \int_\Omega ((z^{(j)} - c_1^{(j)^{US}})^2 - (z^{(j)} - c_2^{(j)^{US}})^2) u^{(j)} d\mathbf{x} \tag{10}
$$

where N_1 is the number of ground truth labels available, and N is the total number of images.

Architecture: The network architecture is outlined in Fig. 1. The network takes in an image, z, of size 256×256 and a binary mask of the same size, which is defined using the user input $\mathcal{M}$. We use a U-Net [16] like structure, in which convolutional layers are applied to both the image and mask separately downwards. At the bottleneck, we join the two separate paths together using a dot product, and then have a single upward path, outputting a segmentation result of the same size as the input. U-Net [16] is a popular architecture for semantic segmentation, as it is able to extract both low level abstract information from the initial layers, and high level abstract information from the final layers, resulting in a fine and accurate prediction.
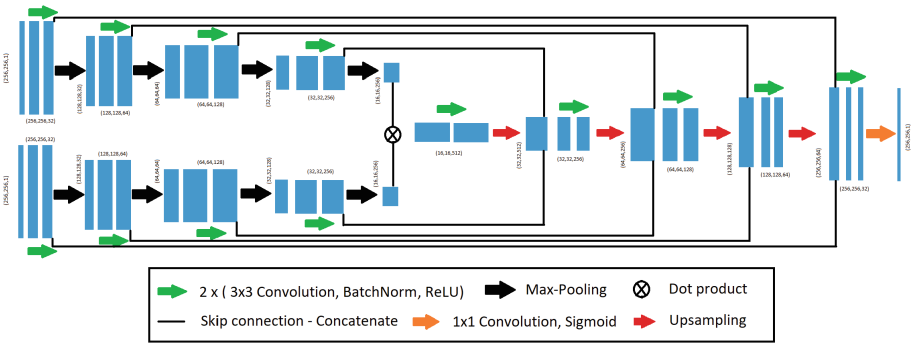

Fig. 1. Structure of our network with two downward paths.

Dataset: We make use of the Liver Tumour Segmentation Benchmark (LiTS) [2], which provides image data and ground truth labels for both the liver and lesions on the liver. We focus on only segmenting the lesions for the application of our algorithm. We used a total of 1552 images, resizing them to 256×256 and using only slices in the database that contained a Liver tumour. We made use of 70%, 15%, 15% of the data in the training, validation and test sets respectively.

Our network requires an initial mask (the polygon formed by $\mathcal{M}$), which for the classical approach usually is gathered via a user clicking on the target object. In order to save us from clicking on each image individually, we use the regions defined in the ground truth and shrink them. These shrunk regions then define our mask, which effectively simulates a user clicking on a small region inside each object.

5   Numerical Results

(a) Input $\mathcal{M}$.   (b) **R-C** model.   (c) Ours.   (d) Ground truth.

(e) Input $\mathcal{M}$.   (f) **R-C** model.   (g) Ours.   (h) Ground truth.

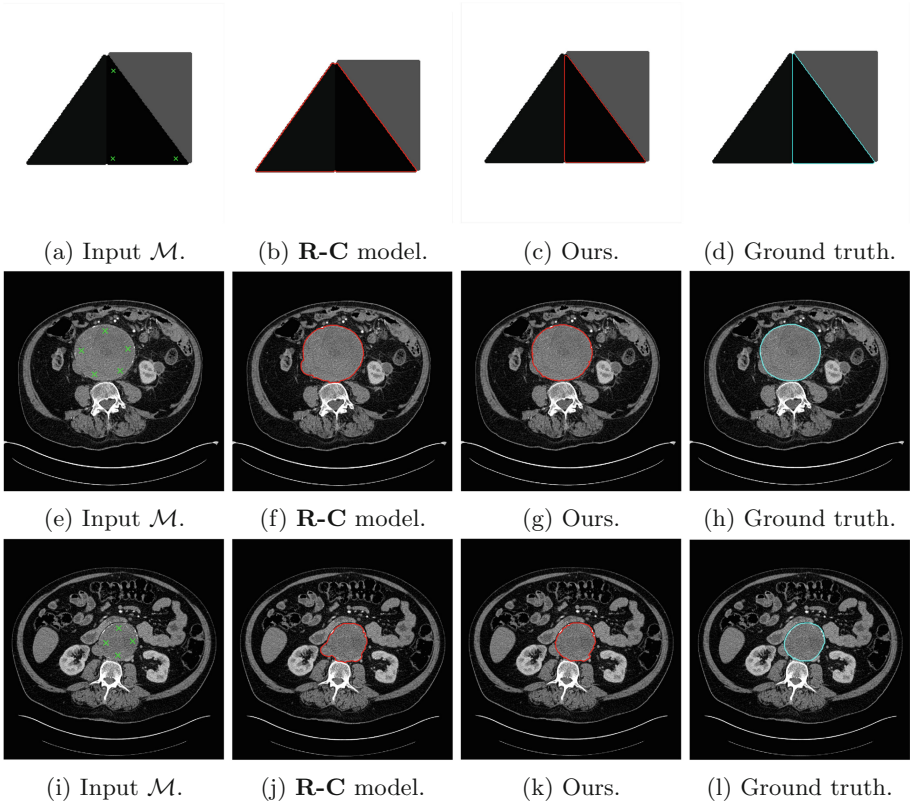(i) Input $\mathcal{M}$.   (j) **R-C** model.   (k) Ours.   (l) Ground truth.

Fig. 2. Results of some low contrast images solved in the variational setting (non DL). Clearly for objects of low contrast, our method provides an improvement over the **R-C** model, as the **R-C** model is unable to detect an edge.

We begin by looking at some results from the model solved in the variational setting, and aim to compare our method against the Roberts-Chen (**R-C**) method [15]. Figure 2 shows three examples. The first is a synthetic image to clearly demonstrate the advantages of ours over **R-C**. The triangle in the middle selected by $\mathcal{M}$ has intensity 0, whereas the intensity to the left has intensity roughly 0.05. The geodesic distance alone is unable to put a penalty on the left triangle, thus the **R-C** method fails to segment the selected triangle. With area constraints introduced, our method clearly is an improvement, able to segment the middle triangle.

The middle and bottom row of Fig. 2 show medical examples of an aneurysm of the abdominal aorta. The data was acquired from the Royal Liverpool Hospital and ground truth labels were provided for comparison. Segmenting the

abdominal aorta is challenging due to regions of low contrast, as objects touching the aorta often have similar intensity. It is clear to see our method successfully prevents the segmentation result from leaking onto nearby objects of similar intensity.

We now examine results from the DL setting, moving focus to the previously discussed LiTS dataset. Figure 3 show some results of the LiTS dataset using our model from a variety of different approaches, namely: classically solving as discussed in Sect. 3, deep learning approaches in the unsupervised, semi-supervised and supervised settings. We also present a table of quantitative results in Table 1, which shows the time and associated DICE score for each example and each method of solving. We see from the table that while the variational method of solving provides good results, it is both time consuming to solve and tune suitable parameters. The deep learning approaches provide an exponentially faster method of solving and offer better results in the supervised and semi-supervised setting.

Table 1. Quantitative results from the examples shown in Fig. 3.

	Variational	Unsupervised	Semi-supervised	Supervised
Time (s)	27.84	0.33	0.42	0.29
DICE	0.886	0.846	0.976	0.997
Time (s)	13.52	0.30	0.34	0.38
DICE	0.638	0.562	0.881	0.790
Time (s)	80.59	0.33	0.33	0.36
DICE	0.906	0.855	0.985	0.997
Time (s)	73.80	0.29	0.33	0.29
DICE	0.919	0.739	0.979	0.977

Table 2 shows the mean and standard deviation DICE score from the entire test set, for each of the approaches plus two common other approaches. We compare with a standard U-Net, one of which uses DICE in the loss, the other uses binary crossentropy - two popular losses for semantic segmentation. We see that using our adjusted architecture and loss provides improved results from the standard approaches.

It is clear to see that the supervised algorithm provides the best results for the segmentation of lesions, and therefore is the algorithm we recommend if ground truth labels are available. As acquiring ground truth labels by experts is often difficult, our unsupervised (or semi-supervised if limited ground truth is available) algorithm is sufficient at producing good results.
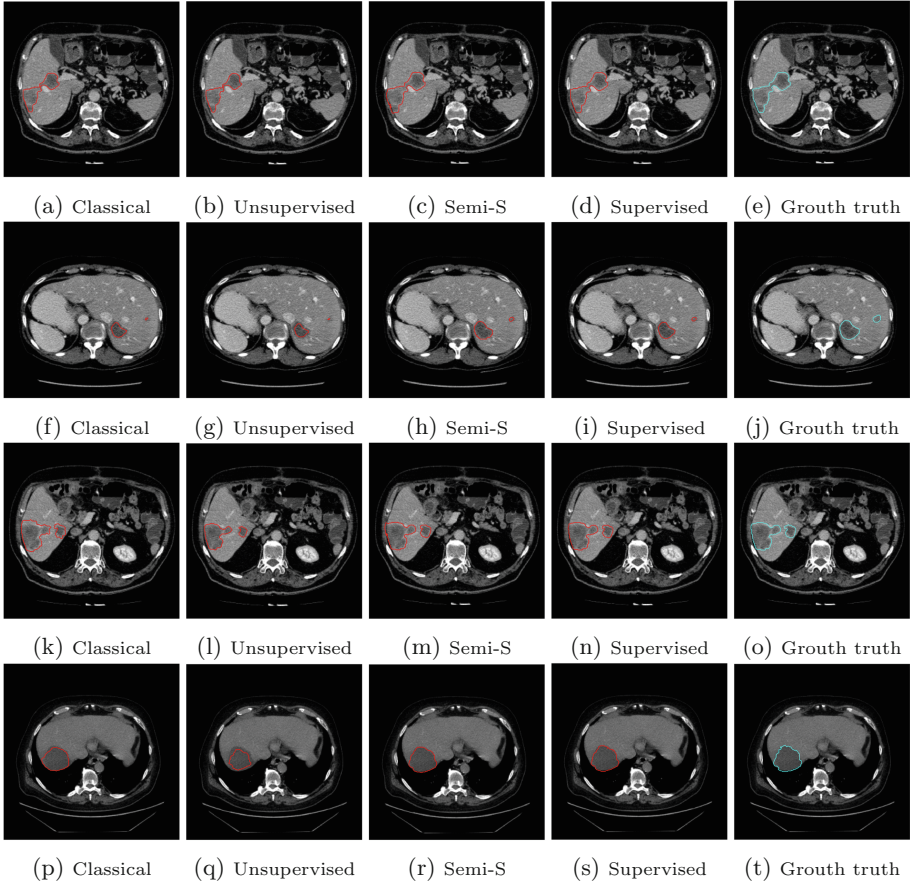
(a) Classical	(b) Unsupervised	(c) Semi-S	(d) Supervised	(e) Grouth truth
(f) Classical	(g) Unsupervised	(h) Semi-S	(i) Supervised	(j) Grouth truth
(k) Classical	(l) Unsupervised	(m) Semi-S	(n) Supervised	(o) Grouth truth
(p) Classical	(q) Unsupervised	(r) Semi-S	(s) Supervised	(t) Grouth truth

Fig. 3. A collection of results using our test data from the LiTS dataset. We have the variational model solved using AOS2 on the far left, the next column shows the output of our unsupervised model, the middle column shows the semi-supervised (semi-s) model, fourth column shows results from our fully supervised model, and the final column shows the ground truth labels.

Table 2. Quantitative results from the whole of the test set, showing the mean and standard deviation of DICE score.

	Unsupervised	Semi-sup	Supervised	U-Net (DICE)	U-Net (Cross-entr.)
Mean	0.671	0.851	0.876	0.552	0.530
Std Deviation	0.305	0.198	0.219	0.347	0.340

6   Conclusion

We have presented a fully convex model for selective segmentation, which is effective when identifying regions of interest in which low contrast is present.

We have shown how to solve it in the classical variational setting and also presented a deep learning version, in which we use the functional in the loss function of a network. The deep learning approach can be implemented in either a supervised, unsupervised or semi-supervised setting, allowing for flexibility in the case of no or some available ground truth labels. All three implementations are useful, depending on data availability. In addition, we have demonstrated how our variational model outperforms previous models, particularly for images of low contrast.

References

1. Badshah, N., Chen, K.: Image selective segmentation under geometrical constraints using an active contour approach. Commun. Comput. Phys. **7**(4), 759 (2010)
2. Bilic, P., et al.: The liver tumor segmentation benchmark (LiTS). arXiv preprint arXiv:1901.04056 (2019)
3. Burrows, L., Guo, W., Chen, K., Torella, F.: Edge enhancement for image segmentation using a RKHS method. In: Zheng, Y., Williams, B.M., Chen, K. (eds.) MIUA 2019. CCIS, vol. 1065, pp. 198–207. Springer, Cham (2020). https://doi.org/10.1007/978-3-030-39343-4_17
4. Caselles, V., Kimmel, R., Sapiro, G.: Geodesic active contours. Int. J. Comput. Vis. **22**(1), 61–79 (1997)
5. Chan, T.F., Esedoglu, S., Nikolova, M.: Algorithms for finding global minimizers of image segmentation and denoising models. SIAM J. Appl. Math. **66**(5), 1632–1648 (2006)
6. Chan, T.F., Vese, L.A.: Active contours without edges. IEEE Trans. Image Process. **10**(2), 266–277 (2001)
7. Chen, X., Williams, B.M., Vallabhaneni, S.R., Czanner, G., Williams, R., Zheng, Y.: Learning active contour models for medical image segmentation. In: Proceedings of the IEEE Conference on Computer Vision and Pattern Recognition, pp. 11632–11640 (2019)
8. Gout, C., Le Guyader, C., Vese, L.: Segmentation under geometrical conditions using geodesic active contours and interpolation using level set methods. Numer. Algorithms **39**(1–3), 155–173 (2005)
9. Jumaat, A.K., Chen, K.: A reformulated convex and selective variational image segmentation model and its fast multilevel algorithm. Numer. Math. Theory Methods Appl. **12**(2), 403–437 (2019)
10. Kass, M., Witkin, A., Terzopoulos, D.: Snakes: active contour models. Int. J. Comput. Vis. **1**(4), 321–331 (1988)
11. Lu, T., Neittaanmaki, P., Tai, X.-C.: A parallel splitting-up method for partial differential equations and its applications to Navier-stokes equations. ESAIM Math. Model. Numer. Anal. **26**(6), 673–708 (1992)
12. Mumford, D., Shah, J.: Optimal approximations by piecewise smooth functions and associated variational problems. Commun. Pure Appl. Math. **42**(5), 577–685 (1989)
13. Osher, S., Sethian, J.A.: Fronts propagating with curvature-dependent speed: algorithms based on Hamilton-Jacobi formulations. J. Comput. Phys. **79**(1), 12–49 (1988)
14. Rada, L., Chen, K.: Improved selective segmentation model using one level-set. J. Algorithms Comput. Technol. **7**(4), 509–540 (2013)

15. Roberts, M., Chen, K., Irion, K.L.: A convex geodesic selective model for image segmentation. J. Math. Imaging Vis. **61**(4), 482–503 (2019)
16. Ronneberger, O., Fischer, P., Brox, T.: U-Net: convolutional networks for biomedical image segmentation. In: Navab, N., Hornegger, J., Wells, W.M., Frangi, A.F. (eds.) MICCAI 2015. LNCS, vol. 9351, pp. 234–241. Springer, Cham (2015). https://doi.org/10.1007/978-3-319-24574-4_28
17. Sethian, J.A.: Fast marching methods. SIAM Rev. **41**(2), 199–235 (1999)
18. Spencer, J., Chen, K.: A convex and selective variational model for image segmentation. Commun. Math. Sci. **13**(6), 1453–1472 (2015)
19. Weickert, J., Romeny, B.T.H., Viergever, M.A.: Efficient and reliable schemes for nonlinear diffusion filtering. IEEE Trans. Image Process. **7**(3), 398–410 (1998)
20. Zhao, H.: A fast sweeping method for Eikonal equations. Math. Comput. **74**(250), 603–627 (2005)